Climate Dynamics
https://doi.org/10.1007/s00382-020-05488-9

Effects of perturbation type on tropical cyclone size over tropical North Western Pacific and Atlantic

Chen Ma[1] · **Tim Li**[1,2]

Received: 3 December 2019 / Accepted: 3 October 2020

Abstract
In authors' previous studies, the role of distinctive mean states in the western North Pacific (WNP) and North Atlantic (NA) in affecting tropical cyclone (TC) size was investigated. In this study, the effect of different synoptic scale perturbation types in the two basins on TC size is further investigated. Numerical model experiments with an initial synoptic wave train (SWT) and easterly wave (EW) environmental condition show that the former (latter) leads to the development of a larger (smaller) TC at an equilibrium state. The physical mechanism responsible for the difference is revealed. Compared with the EW, the surface wind speed of the SWT is larger. Therefore, the SWT generates more moisture in the outer region than EW through surface evaporation process. This favors the development of stronger convection in the outer region. The enhanced convection leads to greater diabatic heating, which lower the local sea level pressure (SLP), which changes surface radial pressure gradients in the inner-core and outer-core of the vortex. On the one hand, the falling of the SLP decreases the surface radial pressure gradient in the inner-core. As a result, the radial wind is weakened and then the radius of maximum wind (RMW) extends outwards after initial contraction. On the other hand, the lower SLP increases the radial pressure gradient in the outer region, strengthening the radial wind outside. The wind convergence favors stronger development of convection in the outer region. Through this positive feedback, inflow in the outer region is further strengthened. This accelerates local tangential wind and thus enlarges the TC size.

Keywords Tropical cyclone size · Synoptic scale perturbation

1 Introduction

Tropical cyclone (TC) is a kind of natural disaster that can cause heavy damage to human life and property (Pielke et al. 2008; Peduzzi et al. 2012). There were a number of studies about the intensity and track of the TC in the past. However, the destructive power of a TC is not only related to the intensity, but also has a lot to do with the size of the TC (Chan and Chan 2018; Hill and Lackmann 2009; Sun et al. 2017). Different from the widely used power dissipation index (PDI) proposed by Emanuel (2005), Sun et al. (2017) defined an index of size-dependent destructive potential (PDS) to account for the effect of the TC size. Ma et al. (2019a) compared the model convergence of the simulated PDI and PDS under different model resolution and cumulus parameterization. It was found that the simulated PDI and PDS have the opposite trends, which means the impact of the TC size on TC destructive potential assessment is very important.

Due to the lack of historical observational data of the TC size, the understanding on the TC size has been lagging behind that of the track and intensity (Ma et al. 2019a). Previous studies shows that the angular momentum transport, the eyewall replacement cycle, the environmental humidity, initial vortex size and sea surface temperature can affect TC size (Chan and Chan 2013; Wang 2012; Hill and Lackmann 2009; Rotunno and Emanuel 1987; Xu and Wang 2010; Sun et al. 2017). The climatology of TC

✉ Tim Li
timli@hawaii.edu

[1] Key Laboratory of Meteorological Disaster, Ministry of Education (KLME), Joint International Research Laboratory of Climate and Environmental Change (ILCEC), Collaborative Innovation Center On Forecast and Evaluation of Meteorological Disasters (CIC-FEMD), Nanjing University of Information Science and Technology, Nanjing, China

[2] International Pacific Research Center and Department of Atmospheric Sciences, School of Ocean and Earth Science and Technology, University of Hawaii, Honolulu, HI, USA

Published online: 10 October 2020

sizes over western North Pacific (WNP) and North Atlantic (NA) has been studied. Whether the statistical data comes from the satellite or the best track data, the results are that the mean TC size on the WNP is larger than that on the NA (Merrill 1984; Chavas and Emanuel 2010; Chan and Chan 2012; Ma et al. 2019b). The reason behind this observation phenomenon has been analyzed in Ma et al. (2019b). Their result indicated that the mean background state of WNP is more beneficial to the TC development than that of NA. Compared with the impact of wind field and moisture, the most dominant contribution comes from the difference of vertical temperature profile on these two basins. The vertical temperature difference on the WNP is larger which is conducive to the development of a stronger TC, and thus make the TC size lager.

However, previous studies showed that the relationship between the TC size and the TC intensity is nonlinear (Wu et al. 2015; Hill and Lackmann 2009). Hill and Lackmann compared the satellite image of Hurricanes Charley (2004) and Floyd (1999). These two hurricanes have the similar estimated maximum near-surface winds of 55 m s^{-1} but their size are very different. Guo and Tan (2017) proposed the TC fullness, a new concept, to describe the complicated relationship between the TC intensity and TC size. These conclusions and observational evidence motivate us to further study the causes of TC size difference between WNP and NA. In our view, apart from the difference in the TC intensity caused by the background state differences, there may be another different physical mechanism affecting the TC size over these two basins.

Different from our previous work (Ma et al. 2019b), here we focus on the synoptic scale perturbation difference between these two basins. While the summer mean background state provides a favorable environmental condition for the TC genesis over these two basins (Gray 1968), it is synoptic scale disturbances that trigger the TC formation (Li 2012; Xu et al. 2014). Most of the precursor disturbance over the NA is African easterly waves (EW) (Burpee 1972; Landsea 1993; Avila 1991; Avila and Pasch 1995; Peng et al. 2012). Different from the NA, the types of TC precursor signals are relatively complex over the WNP. Precursor perturbations in the WNP include TC energy dispersion induced Rossby wave train (Li et al. 2003, 2006; Li and Fu 2006), northwest-southeast oriented synoptic wave train (SWT) (Li 2006; Fu et al. 2007, 2012), and Pacific easterly wave (Chang et al. 1970; Ritchie and Holland 1999). The SWT is the most frequent type among these three precursor perturbations (Lau and Lau 1990; Fu et al. 2007; Xu et al. 2013; Yuan et al. 2015). Since the SWT and EW are the most dominant synoptic scale perturbation type of TC formation over the WNP and NA, what is the structure difference between the SWT and EW? How does this perturbation difference affect the final TC size?

The rest of this paper is organized as follows. The model configuration, the comparison of the structure between the SWT and EW, experimental design are given in Sect. 2. In Sect. 3, we examine the effect of the SWT and EW on the TC size. The possible physical mechanism through which the synoptic perturbation affects the TC size is examined with additional experiments in Sect. 4. Finally, major findings of the study are summarized and discussed in Sect. 5.

2 The model and experiment design

2.1 Model configuration

In this study, the Advanced Research Weather Research and Forecasting (WRF-ARW) system version 3.7 is employed for the numerical experiments (Skamarock et al. 2008). Three nested domains with the two inner nests having two-way interactions are constructed. For all the experiments in the WNP and NA, the horizontal resolution of 27, 9 and 3 km have domain sizes of 301×251, 301×301, and 301×301 grid points for the three meshes, respectively. The model has 37 layers in the vertical with a model top at 50 hPa. The Kain–Fritch convective scheme (Kain and Fritsch 1993) is applied to the two outermost meshes and the Lin microphysics scheme (Lin et al. 1983) is used in all meshes. Other model physics include the Yonsei University (YSU) planetary boundary layer (PBL) scheme, thermal diffusion land surface scheme, and Monin–Obukhov surface-layer scheme (Hong et al. 2006). A fixed lateral boundary condition is used for the outermost domain and the two inner nested domains move automatically following the simulated TC (Davis et al. 2008). To simplify the interpretation of the results, the land is removed and set to include only water. The SST of the whole domain is a constant of 29 °C.

2.2 Initial synoptic perturbations in WNP and NA: SWT vs. EW

The large-scale synoptic perturbations anomaly fields of WNP and NA are derived from the National Centers for Environmental Prediction (NCEP) reanalysis data (Kalnay et al. 1996). Our data covers the period 1 July—30 September, from 2001 to 2010. First, a multivariate empirical orthogonal function (MEOF) analysis is performed onto the 3–8 day filtered zonal wind and vorticity fields over these two basins. Figure 1 shows the horizontal patterns of the first and second EOF modes of the synoptic scale wind field on the WNP and NA. The EOF-1 and EOF-2 patterns represent different propagation phase of the SWT and EW. In the horizontal direction, the SWT has a typical northwest-southeast oriented structure and the wavelength is about 2000 km. The center of the maximum vorticity of the SWT

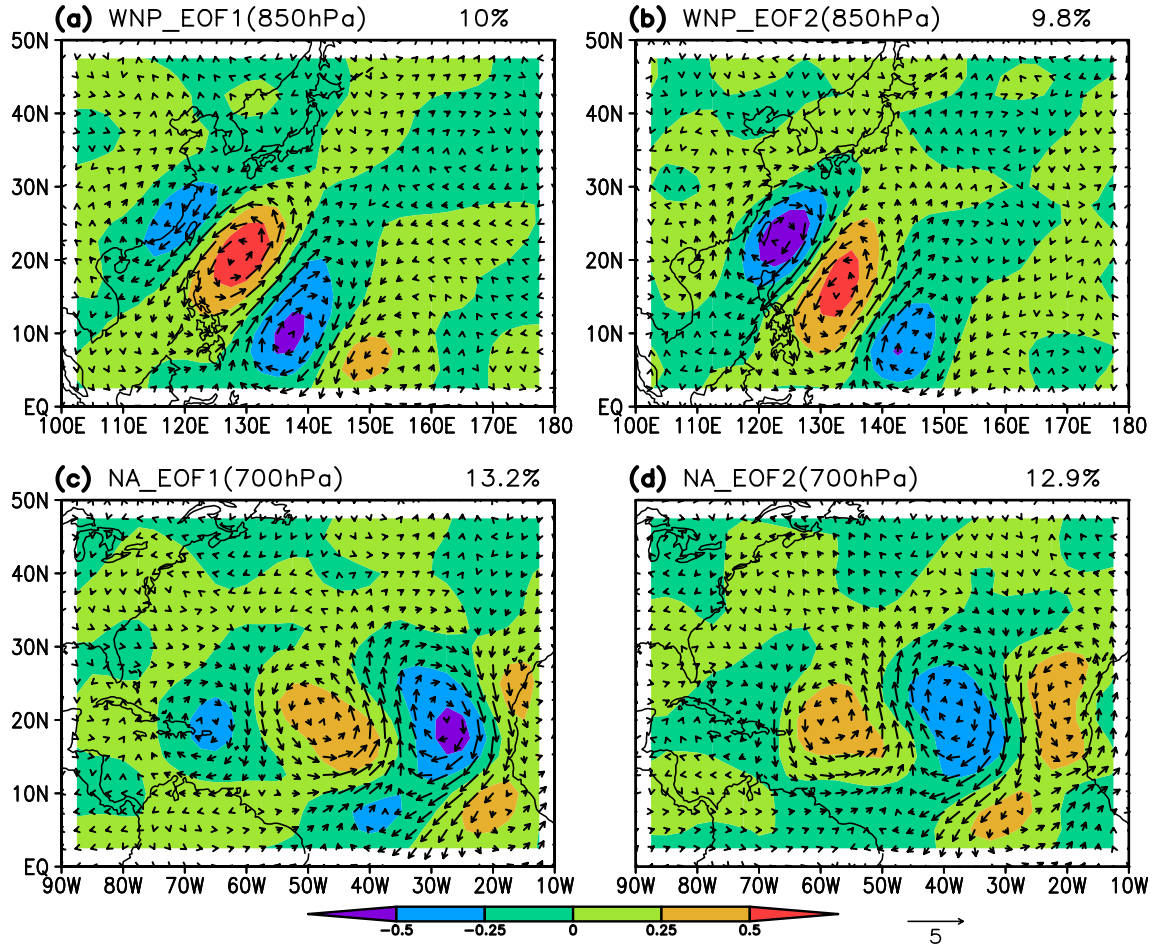

Fig. 1 The horizontal patterns of the first (left) and second (right) EOF modes of the 3–8-day filtered wind (vector, m s^{-1}) and vorticity (shaded, 10^{-5} s^{-1}) fields in **a**, **b** WNP and **c**, **d** NA derived from the FNL data. The number in the upper right corner of each panel is the variance explained by each EOF mode. The EOF analysis was done at maximum variability levels, 850 hPa for WNP and 700 hPa for NA, respectively

in EOF-1 at 850 hPa is located at 20° N. For the EW over the NA, it is more zonally oriented, and the wavelength is about 3000 km. The latitude of the maximum vorticity center of the EW in EOF-1 at 700 hPa is at about 20° N as well. Then, using positive and negative two standard deviation of the time series of the EOF as a threshold, 51 (40) SWT (EW) cases are selected for a composite analysis to derive the evolution of SWT and EW patterns. The reason to use two standard deviations is that we want the composite SWT or EW to be stronger. As shown in previous studies, not all SWT or EW can develop into a TC. Peng et al. (2012) and Fu et al. (2012) indicated that the ratio between developing and non-developing disturbances for TC formation is about 1:2 and 1:1 over NA and WNP, respectively. In addition, Fu et al. (2007) investigated thirty-four TC genesis events over WNP in the boreal summers of 2000 and 2001. Their results show that about 30% of TC formation relate to SWT. In other words, the frequency that SWT evolves into a TC in the boreal summer is about five cases per year. From this perspective, the composite of two standard deviations is more reasonable.

Figure 2 shows the vertical profile of area-averaged (1300 km × 1300 km) vorticity, divergence, specific humidity and temperature centered in the maximum vorticity area for the SWT and EW. Compared with the EW, the vorticity of SWT is larger from the surface to the 300 hPa (Fig. 2a). It is worth mentioning that the maximum vorticity is located on 850–900 hPa for SWT and 600–700 hPa for EW. This means the SWT is a bottom type vortex and the EW is a middle level vortex. Ge et al. (2013) pointed out that the bottom vortex is more favorable for the TC genesis and development. The divergence in Fig. 2b indicated that the SWT has strong ascending motion. The ascending motion of SWT may favor the genesis and development of a TC. Meanwhile, the specific humidity profile in Fig. 2c shows that the SWT has more abundant moisture than EW for each vertical layer.

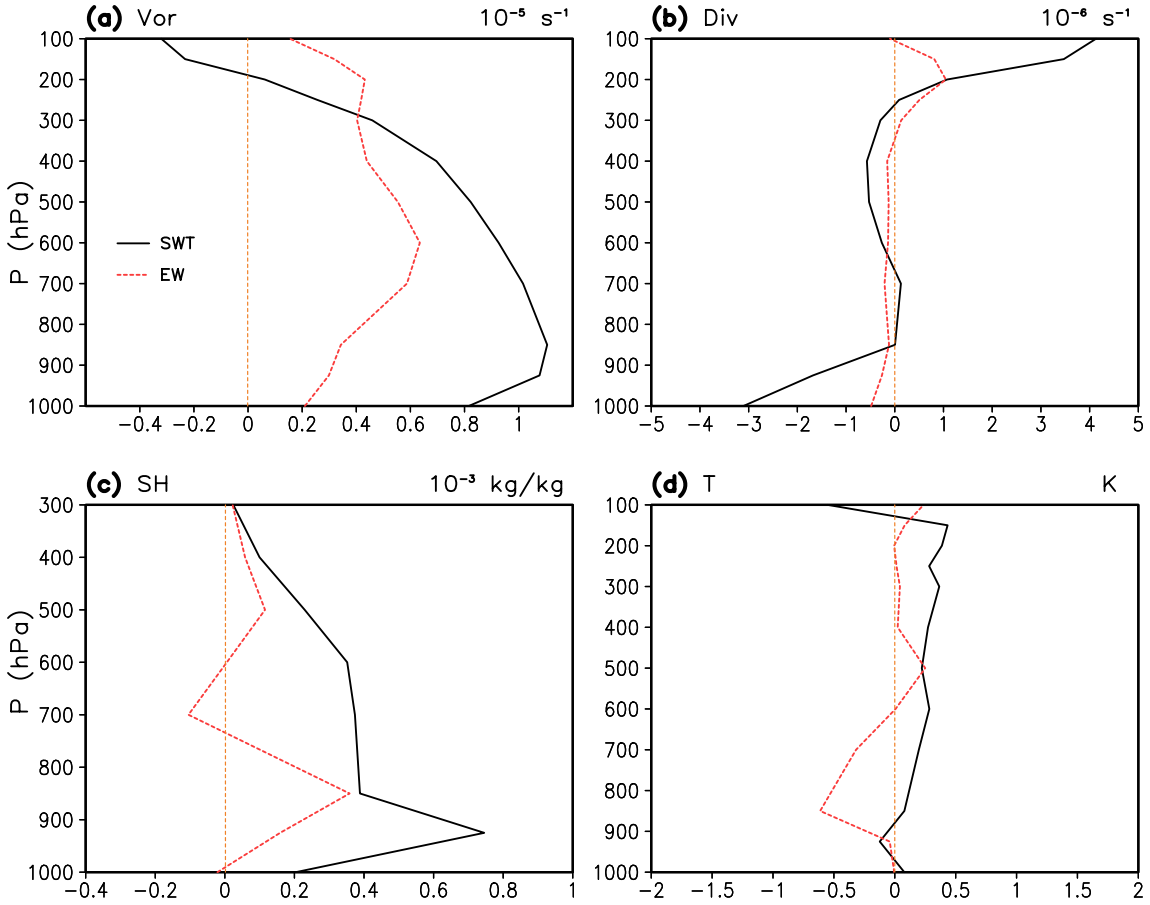

Fig. 2 The vertical profiles of area-averaged (1300 km × 1300 km) **a** vorticity (10^{-5} s^{-1}), **b** divergence (10^{-6} s^{-1}), **c** specific humidity (g kg^{-1}) and **d** temperature (K) anomaly fields centered at the maximum vorticity for the SWT (black solid line) and EW (red dashed line) composites

For the temperature anomaly profile in Fig. 2d, the EW has a negative anomaly around 850 hPa level. By examining the vertical profile of the temperature associated with SWT and EW, we note that the vertical temperature difference between the upper and lower troposphere is small. This implies that the temperature anomaly of SWT and EW has limited influence on the environmental atmospheric static stability.

2.3 Experimental design

To explore the effect of synoptic perturbation type on TC size in different basins, two experiments are designed, one for WNP and the other one for NA, identified as P_SWT and A_EW, respectively (Table 1). The model is set on a beta plane so that the SWT or EW can move slowly

Table 1 List of all experiments. All variables of the SWT and EW are added in the Group 1

Group	Experiment names	Description
Group 1	P_SWT	The model initial and lateral boundary conditions are from the sum of the quiescent background superposed by a composite SWT pattern and an initial vortex
	A_EW	Same as P_SWT except that the composite EW pattern is added instead of SWT pattern
Group 2	SWT_SH	Same as P_SWT except that for the SWT fields, only the moisture field is retained
	EW_SH	Same as A_EW except that for the EW fields, only the moisture field is retained
Group 3	SWT_V	Same as P_SWT except that for the SWT fields, the moisture field is removed
	EW_V	Same as A_EW except that for the EW fields, the moisture field is removed

The SH in Group 2 is the specific humidity of the synoptic scale perturbations. The V in Group 3 is the dynamic field, including the wind field, temperature, geopotential height and SLP of the synoptic scale perturbations

northwestward. The wavelength of the synoptic perturbation is typically in the range of 2000–3000 km. Therefore, the model domain should be large enough to cover the movement of SWT and EW. The experiments domain here cover an area of 0°–50°N, 100°–160°E for P_SWT and 0°–50°N, 30°–90°W for A_EW, respectively. Since we focus on the effect of different synoptic scale perturbation type on the TC size, the background environment flow is set to be quiescent. The relative humidity and temperature are horizontally uniform and the vertical profile of January-mean observations at Willis Island (Holland 1997) is applied. In addition, the SST of the whole domain is a constant of 29 °C.

Then, the 10-year composite summer synoptic scale perturbation of WNP and NA including variables such as surface pressure, wind fields, geopotential height, temperature, SST, and specific humidity are added to the quiescent environment. Previous studies pointed that the synoptic scale wave (i.e., SWT and EW) can represent a quasi-closed region of recirculating horizontal flow and protect the proto vortex from the hostile exterior influences before the proto vortex develop into a TC (Dunkerton et al. 2009; Wang et al. 2012). In other words, the SWT and EW provide a favorable environment for TC formation. An initial weak vortex is added as a seed disturbance over the center of SWT and EW, respectively.

The radial and vertical profiles of the tangential wind of the initial vortex used here is (Wang 1995):

$$V_t(r,\sigma) = \begin{cases} \sin\left[\frac{\pi}{2}\left(\frac{\sigma-0.1}{1-0.1}\right)\right]\frac{V_m}{r_m}\left(e^{\left(1-\frac{r}{r_m}\right)} - \frac{|r-r_m|}{r_0-r_m}e^{\left(1-\frac{r_0}{r_m}\right)}\right) & \sigma > 0.1 \\ 0 & \sigma \le 0.1 \end{cases}$$

where r is the radial distance from the vortex center, r_m the radius of maximum tangential wind, V_m the maximum tangential wind at r_m, σ the vertical sigma level and r_0 is 1000 km from the vortex center where the tangential wind decreases to zero. The maximum tangential wind of the initial vortex is 15 m s^{-1} at the radius of 150 km at the surface. The same initial vortex is specified so that one can focus on examining the effect of the SWT and EW on the subsequent vortex development. The wind speed decreases gradually upward. The mass and thermodynamic fields are derived based on the nonlinear balance equation so that the initial vortex satisfies both the hydrostatic and gradient wind balances (Wang 1995, 2001).

In summary, the synoptic scale perturbation and the initial seed vortex are added to the quiescent background as the initial condition of the experiment (Table 1). The lateral boundary conditions are the sum of the synoptic scale perturbation and the quiescent background, varied with time. The model runs for five days and the result can show us the effect of SWT or EW on the TC size.

3 Effects of SWT and EW conditions on TC size

Figure 3 shows the time evolution of the TC intensity and size in the P_SWT and A_EW experiments. As the SWT has more abundant moisture, stronger vorticity and ascending motion (Fig. 2), the initial vortex in the P_SWT develops faster than that in the A_EW. The greater moisture content in the SWT is attributed to a greater wind induced surface evaporation and a greater ascending motion that increases the moisture through vertical advection. Meanwhile, the TCs in two experiments have the similar intensity when TCs reach their mature stage at about hour 96. This is because the atmospheric static stability is similar for the two experiments as the vertical temperature gradients associated with SWT and EW are small (Fig. 2d). In terms of the TC inner-core size (Fig. 3c), the time evolution of the radius of maximum wind (RMW) of P_SWT and A_EW are similar for the first 48 h. After that, the RMW of P_SWT develops to be 40 km larger than that of A_EW at the end of simulation. The outer-core size (Fig. 3d), measured by the radius of the 17 m s^{-1} surface wind speed (R17), is always larger in the P_SWT than A_EW throughout the simulation time. For the first 24 to 48 h, the R17 difference may be caused by the difference of the TC generation time. However, the R17 difference between these two experiments becomes larger at the later time while the TC intensity in these two experiments are similar. This implies that the R17 difference does not depend on the vortex intensity. This continuous growth of R17 and RMW in P_SWT suggests that the outer-core size is closely related to the inner-core size, and there may be positive feedback. The averaged TC size during the last two simulation days is 252 km and 175 km for P_SWT and A_EW, respectively. The size difference of 77 km indicates that the SWT favors a larger TC.

Figure 4 shows the rainfall rate in these two experiments for the first four simulation days. The larger TC outer-core size in P_SWT experiment inferred from the rainfall is consistent with the R17 in Fig. 3d. Meanwhile, after 48 h of the simulation (Fig. 4b, f), the RMW of these two experiments are almost the same as inferred from the precipitation. After that, the RMW of P_SWT increases (Fig. 4c, d), whereas the RMW of A_EW decreases slightly (Fig. 4g, h). Since the initial vortex is the same and the background state is quiescent, the difference between P_SWT and A_EW can only arise from the synoptic scale disturbance. This simulation result indicates that the SWT can develop a larger TC inner-core and outer-core size. Moreover, it is worth mentioning that the P_SWT experiment generates more precipitation in the outer region than the A_EW in the early stage of the simulation. The reason behind this may be the advantage of the dynamic fields and moisture of the SWT.

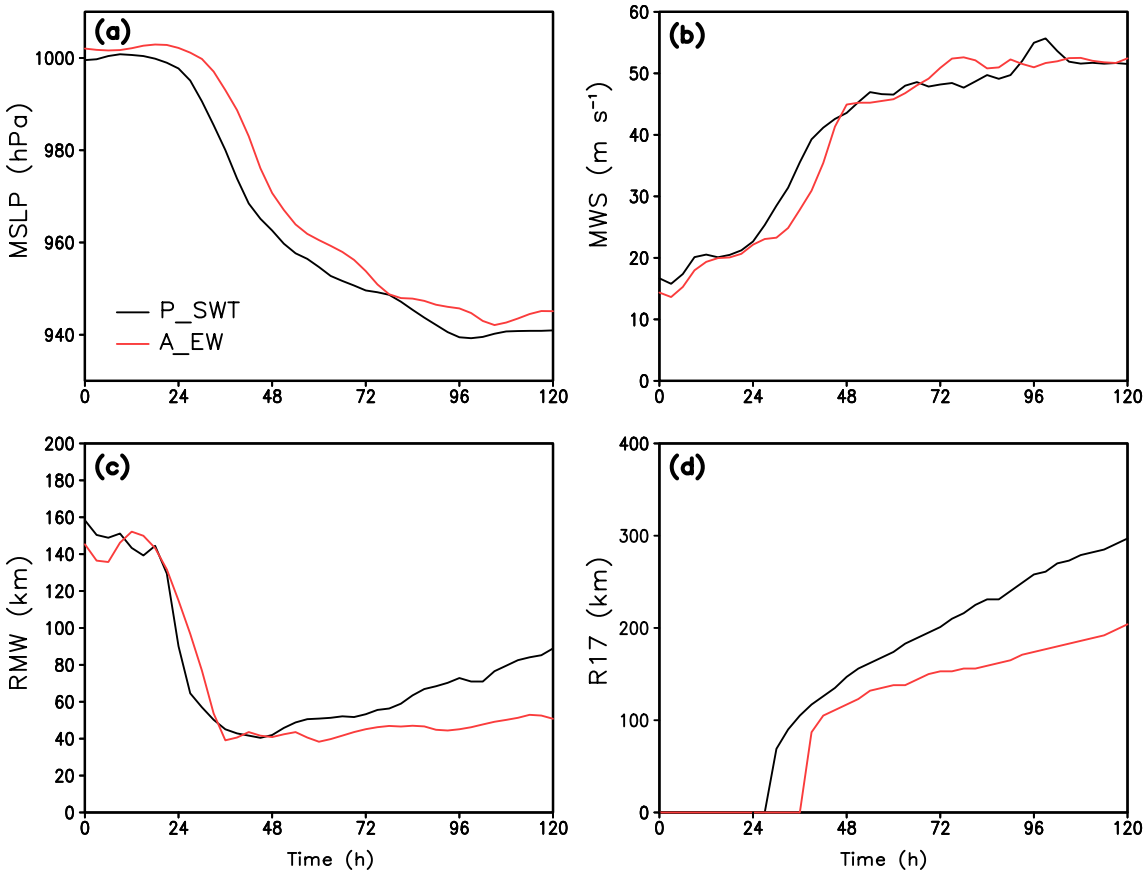

Fig. 3 Time evolutions of **a** MSLP (hPa), **b** MWS (m s^{-1}), **c** RMW (km) and **d** R17 (km) at 10-m height derived from the P_SWT (black line) and A_EW (red line) experiments

4 Physical mechanism for generating the distinctive TC sizes

Ma et al. (2019b) investigated the effect of environmental background state on TC size and pointed out that the summer mean state of the different basin can influence TC size through the change of the TC intensity. However, the results here are quite different. While the simulated TC intensity is similar, the TC size differs remarkably and the TC size change is closely related to the RMW change in the present study.

From the perspective of rainfall rate, the SWT environment is conducive to generating convection in the outer region (Fig. 4). The stronger convection in the outer region causes the release of more diabatic heating. Figure 5 shows the 24-h averaged diabatic heating difference in these two experiments from the initial time to hour 96. The P_SWT has more diabatic heating than A_EW during the early stage of the simulation (Fig. 5i, j). After 48 h, compared with P_SWT experiment (Fig. 5c, d), the diabatic heating in A_EW (Fig. 5g, h) is stronger near the eyewall. However, in the outer region, the opposite is true, that is, the diabatic heating of P_SWT is larger than A_EW. Wang (2009) pointed out that the diabatic heating in active spiral rainbands could lower the surface pressure outside the RMW and change the pressure gradient across the RMW. Since the SWT generates more convection and releases more diabatic heating in the outer region, the surface pressure away from the TC center can be lower, therefore the distribution of the radial pressure gradient can be different from the A_EW. Figure 6 shows the Hovmöller diagram of azimuthal-mean radial pressure gradient at the surface. It can be seen that the position of maximum radial pressure gradient expands outwards continuously in the P_SWT experiment (Fig. 6a), which is consistent with the time evolution of RMW (Fig. 3c). In contrast, the position of maximum radial pressure gradient in A_EW stays fixed. More importantly, compared with the P_SWT experiment, the radial pressure gradient in A_EW is larger in the inner-core at about the radius of 50 km. However, in the outer region, the radial pressure gradient in P_SWT is larger than A_EW (Fig. 6c). The reason behind is that the convection in the outer region releases more diabatic heating and lowers the local surface pressure. Therefore, the distribution of surface radial pressure gradient in the inner core and outer

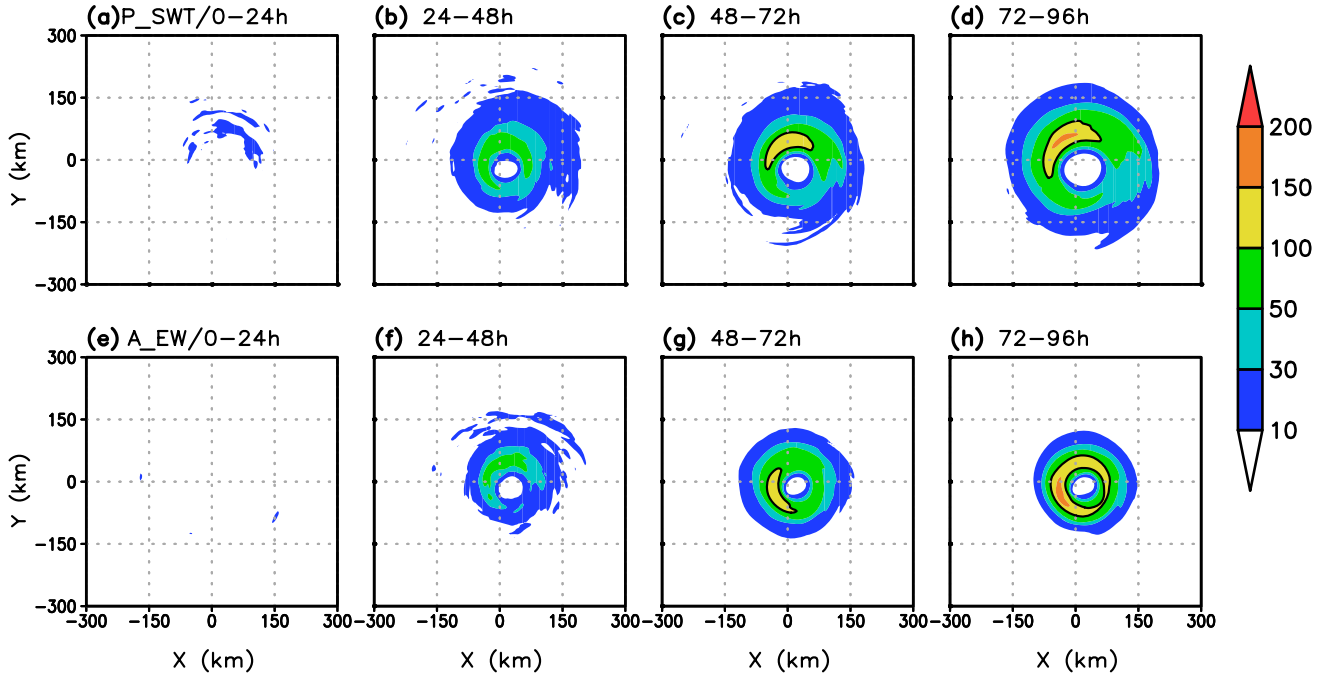

Fig. 4 Horizontal patterns of 24-h averaged rainfall rate (mm h^{-1}) (sum of cumulus and grid scale precipitation) simulated from **a**–**d** the P_SWT and **e**–**h** A_EW experiments

core region is changed. In the inner-core region, the convection in the outer region tends to decrease the local surface pressure gradient. However, in the outer region, it tends to increase the surface radial pressure gradient.

As the surface pressure gradient distribution changes, the radial wind field responds to it according to the radial wind equation, which is expressed as:

$$\frac{du_r}{dt} = -\frac{1}{\rho}\frac{\partial p}{\partial r} + \frac{v_t v_t}{r} + f v_t - D u_r$$

where r is the radial distance from the TC center, u_r and v_t are azimuthal-mean radial and tangential winds, respectively, f is the Coriolis parameter, ρ and p are the air density and pressure, Du_r is parameterized subgrid scale diffusion term which includes friction and horizontal diffusions. Figure 7a–h show the azimuthal and 24-h averaged cross section of the radial wind in the P_SWT and A_EW experiments, respectively. The radial wind difference between P_SWT and A_EW is presented in Fig. 7i–l. It is notable that, if the radial wind speed increases in the inner-core, the TC inner-core size (RMW) will become smaller (Wang 2009). As the surface pressure gradient in A_EW is larger in the inner-core (Fig. 6), the radial wind in A_EW is much stronger (Fig. 7g, h, l), and thus the TC in A_EW has a small RMW. However, for the outer-core size, due to the distribution change of the surface pressure gradient (Fig. 6), the TC radial wind field in the P_SWT experiment extends outwards gradually from 300 to 450 km as the TC develops (Fig. 7b–d). The radial wind difference between P_SWT and A_EW shows that an enhanced convergence occurs in the outer region in the P_SWT experiment (Fig. 7j–l). According to the vorticity equation, the convergence anomaly would generate a cyclonic vorticity tendency $[-(f+\xi)\nabla\cdot\overrightarrow{V_h}]$, where f and ξ are the Coriolis parameter and relative vorticity, respectively, $\nabla\cdot\overrightarrow{V_h}$ is the horizontal wind divergence. As a result, the local tangential wind is enhanced thus the TC outer-core size expands outwards. Significantly different from this, the radial wind range in the A_EW experiment is narrow, even the radial wind speed becomes larger (Fig. 7g, h, l). Compared with the TC in the P_SWT experiment, although the TC in A_EW has stronger inflow at surface and outflow at high level, the spatial distribution is narrow, thus the TC outer-core size is small. The anomalous convergence and the enhanced tangential wind in the P_SWT can further induce local convection through enhanced surface evaporation and boundary layer moisture.

To help understand the physical mechanism behind, a schematic diagram is presented to summarize the reason why the SWT environment can generate a larger TC size (Fig. 8). Compared with the EW environment, the SWT environment generates more convection in the outer region. The convection in the outer region releases more diabatic heating outside, lowering the SLP at the convection position. On the one hand, the falling of the SLP decreases the surface radial pressure gradient in the inner-core. As a result,

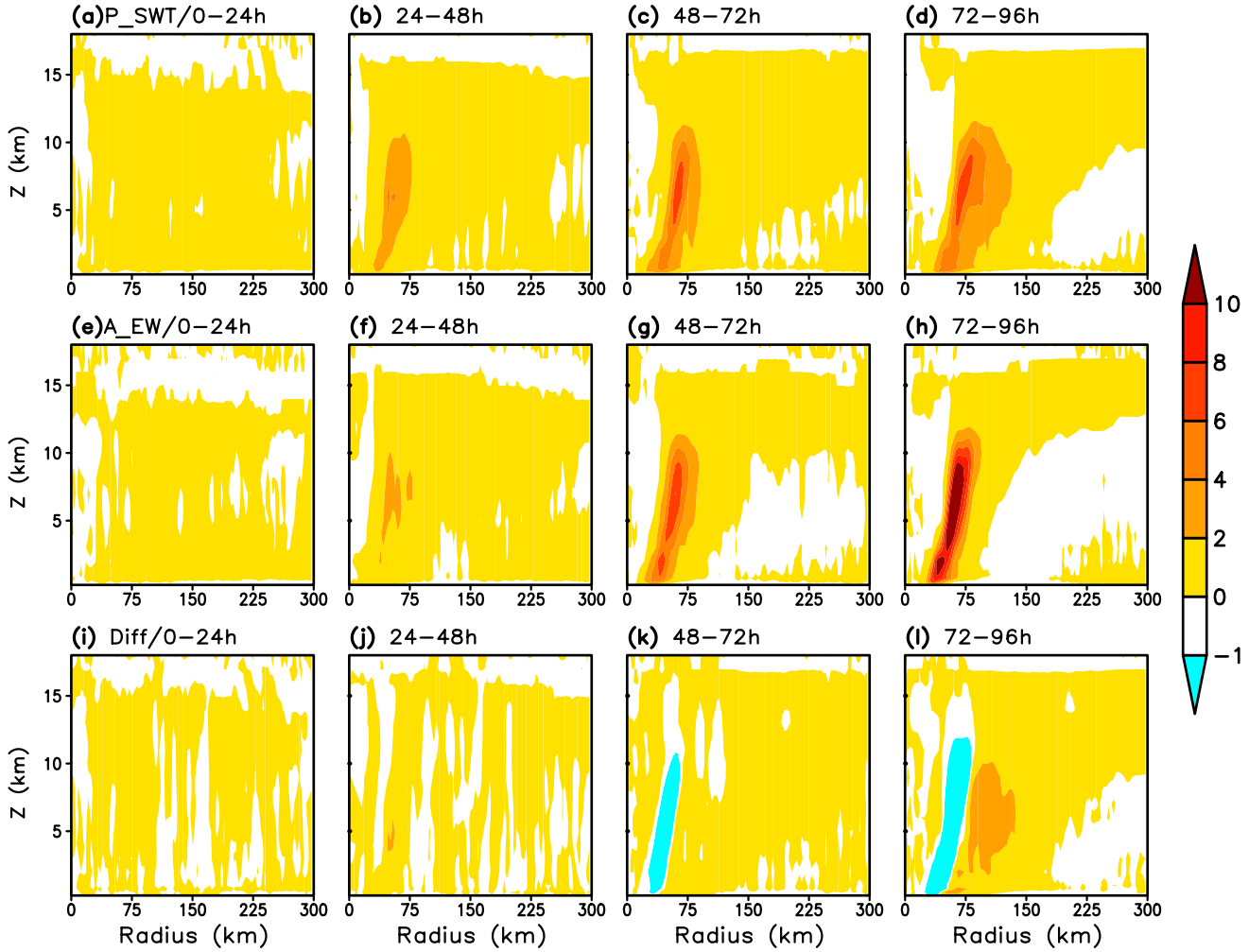

Fig. 5 The vertical-radial cross sections of the azimuthal and 24-h averaged diabatic heating (unit: 10^{-3} K s^{-1}) field from the **a**–**d** P_SWT, **e**–**h** A_EW and **i**–**l** the difference between these two experiments (P_SWT—A_EW)

the radial wind is weakened according to the radial wind balance and the RMW extends outwards. On the other hand, the low SLP in the outer region increases the radial pressure gradient and enhances the radial wind in the outer region. The wind convergence further enhances the local convection and accelerates the inflow in the outer region. Through this positive feedback loop, the local tangential wind increases and extends outwards, leading to a larger TC size (R17).

However, a question still remains, why the SWT environment generates more convection outside. The vertical profile of the SWT and EW (Fig. 2) shows that the vorticity of SWT is larger than EW from the surface to 300 hPa level and the ascending motion is stronger as well. Meanwhile, the SWT has more abundant moisture for the whole vertical layer. The SWT has an advantage in both circulation and moisture field, we wonder which one is dominant to generate convection outside and then enlarge the TC size? To figure out this question, we design another two groups of the sensitivity experiments (Table 1). The group 2 and group 3 are the moisture and circulation experiments, respectively. In the moisture experiments, only the specific humidity from the SWT and EW is added to the quiescent environment as the initial condition; In the circulation experiments, the dynamic fields including wind field, temperature, geopotential height and SLP are added. Through these two sets of experiments, the effect of the moisture and circulation fields from the synoptic scale perturbations on the TC size is distinguished.

Figures 9 and 10 show the time evolution of the TC intensity and size in sensitivity experiments. As we mentioned in Sect. 3, the R17 difference may come from two parts. On the one hand, the TC generation time can cause the TC size difference; on the other hand, the change of the TC structure caused by the surrounding environment may lead to the size difference as well. In moisture experiments, the effect of specific humidity is investigated (Fig. 9). The averaged TC size during the last two simulation days is 185 km and 157 km

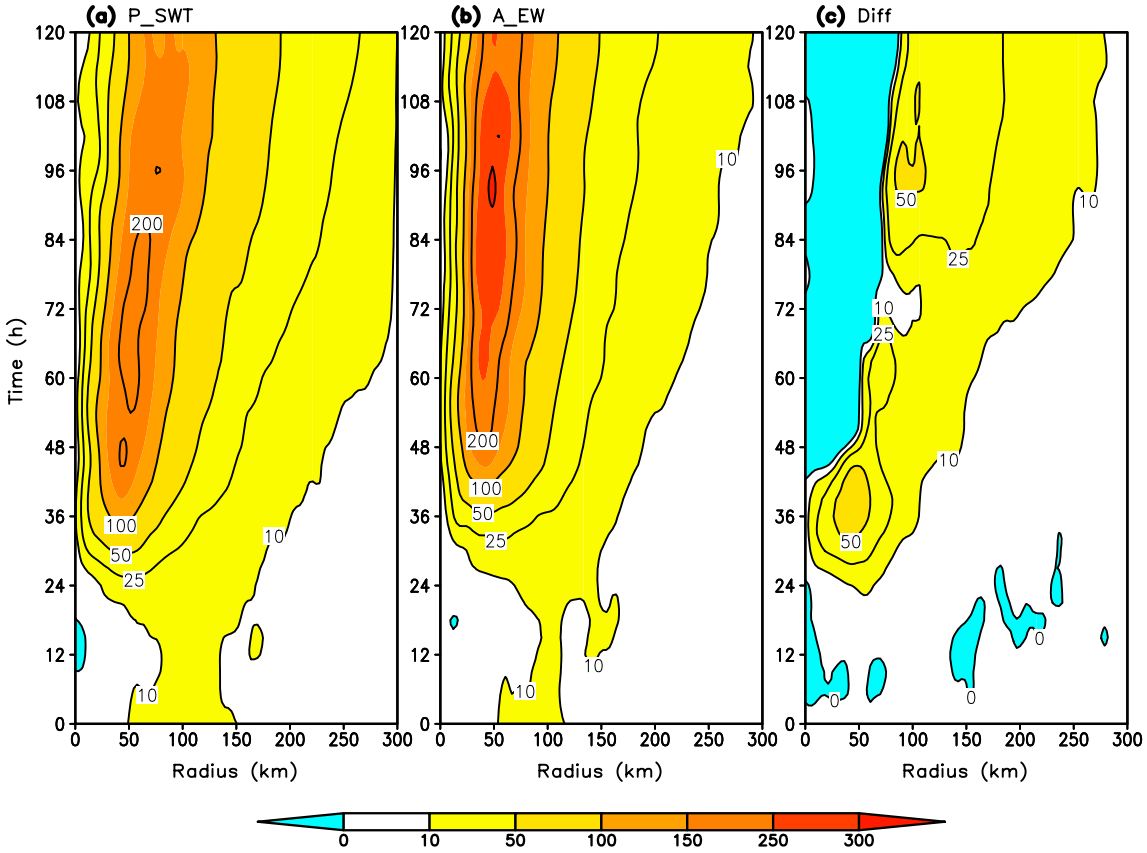

Fig. 6 Hovmöller diagrams of the azimuthal-averaged radial pressure gradient (kg m^{-2} s^{-1} h^{-1}) at the surface for the **a** P_SWT, **b** A_EW and **c** the difference between these two experiments (P_SWT—A_EW)

for SWT_SH and EW_SH, respectively. The size difference is 28 km, accounting for about 40% of the TC size difference in the P_SWT and A_EW. The simulation result shows that the TC in SWT_SH experiment develops earlier (Fig. 9a, b). Therefore, the R17 of SWT_SH appears first (Fig. 9d). After 48 h of the simulation, the RMW of SWT_SH and EW_SH is nearly same (Fig. 9c). In addition, the difference of the R17 between the two experiments does not increase with time. This implies that the environmental specific humidity associated with the SWT and EW influences TC size primarily during the initial TC development stage. However, the circulation experiments exhibit different characteristics. In the circulation experiments, the specific humidity difference is removed, the only difference in the initial condition comes from the circulation fields. In this group, the TC genesis time is similar and the R17 appears at the same time (Fig. 10). As the RMW difference begins to appear at about hour 48, the R17 has a corresponding difference as well. The averaged TC size during the last two days is 232 km and 187 km for SWT_V and EW_V respectively. The size difference in circulation experiment is 45 km, accounting for about 60% of the TC size difference in the P_SWT and A_EW. The simulation results of the moisture and circulation experiments demonstrate that the circulation factor of the synoptic scale perturbation plays a larger part in influencing the TC size.

The initial surface wind of SWT and EW derived from the observational data is presented in the Fig. 11. The wind speed of the SWT is larger than EW in the positive vorticity area at the surface. Therefore, the SWT generates more moisture than EW by evaporation process (Fig. 12). Figure 12 shows the time averaged horizontal distribution of the upward moisture flux from the circulation sensitivity experiments. It can be seen that the SWT_V generates more upward moisture flux due to the strong surface wind and evaporation effect. Meanwhile, there is a high upward moisture flux difference at the radius of 140 km (Fig. 12c). This is the place that the outer region convection develops. Figure 13 shows the time averaged horizontal plot of the specific humidity difference between SWT_V and EW_V at the surface. Although the specific humidity of the SWT_V and EW_V experiments is the same in the initial condition, the specific humidity difference appears gradually as the circulation field of the SWT generates more moisture through the evaporation (Fig. 13c). Meanwhile, the vertical profile of the divergence field indicates that the ascending motion of the SWT environment is stronger (Fig. 2b). Both factors

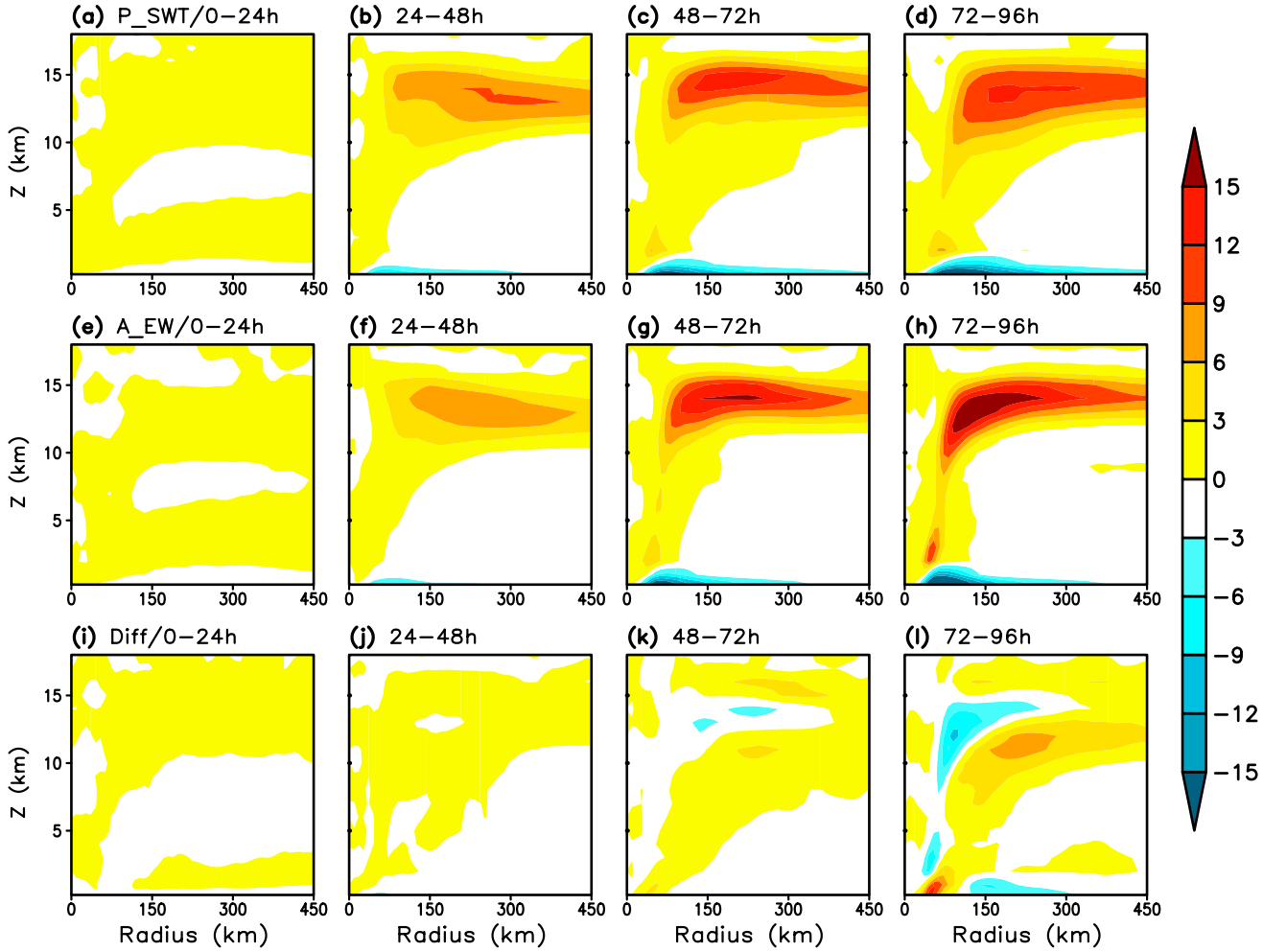

Fig. 7 The vertical-radial cross sections of the azimuthal and 24-h averaged radial wind (m s^{-1}) field derived from the **a**–**d** P_SWT and **e**–**h** A_EW experiments and **i**–**l** their difference (P_SWT—A_EW)

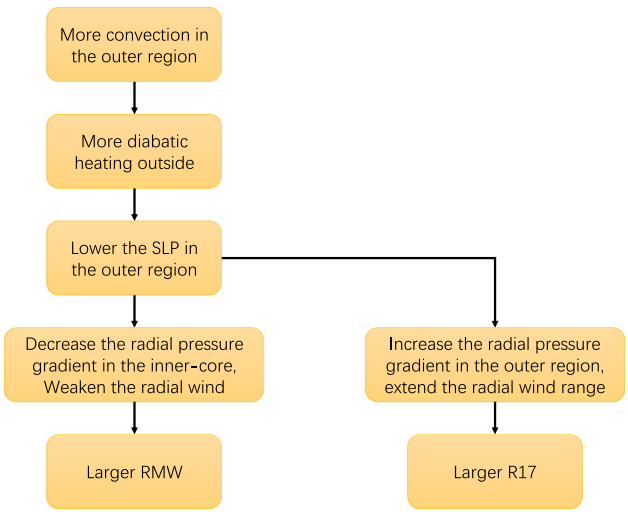

Fig. 8 A schematic diagram summarizing key physical processes through which the SWT environment promotes a larger size TC

promote the development of convection in the outer region, resulting in the increase of the TC size.

5 Summary and discussion

Previous observational studies pointed out the TC size difference between the WNP and NA. Different from Ma et al. (2019b) that focused on the influence of the Pacific and Atlantic mean state on TC size, the effect of dominant synoptic scale perturbation types in the two basins on the TC size is investigated here. A multivariate EOF analysis is applied to derive the SWT and EW patterns. As the most common precursor disturbances on WNP and NA (Fu et al. 2007), the SWT and EW have distinctive horizontal and vertical structures.

The first group of experiments using the SWT and EW as the synoptic environment for an initial weak vortex shows that the SWT environment can produce a larger TC

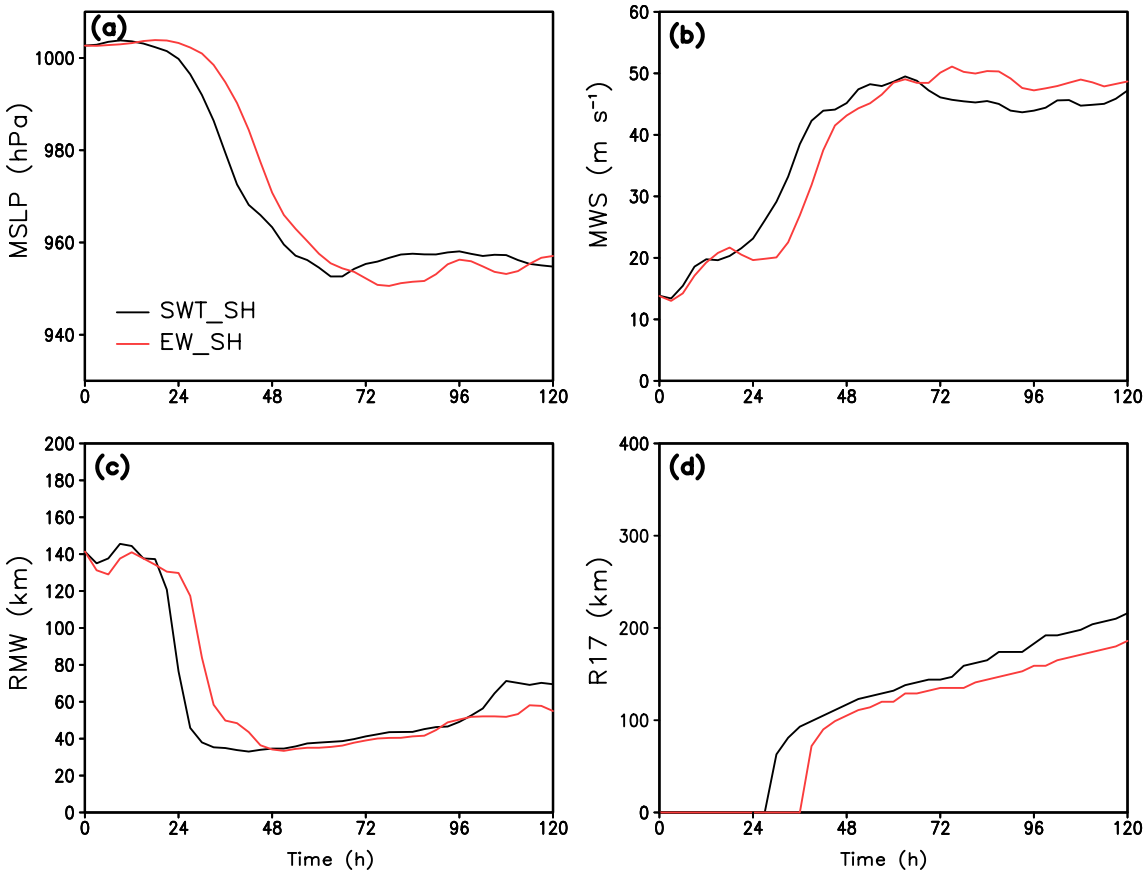

Fig. 9 Time evolutions of **a** MSLP (hPa), **b** MWS (m s^{-1}), **c** RMW (km) and **d** R17 (km) at 10-m height simulated from the SWT_SH (black line) and EW_SH (red line)

inner-core (RMW) and outer-core size (R17). The physical mechanism is further investigated (Fig. 8). It is found that the SWT can generate stronger convection in the outer region. The stronger convection in the outer region causes the release of more diabatic heating, lowering the local SLP. The drop of the SLP in the outer region changes the distribution of the surface radial pressure gradient in the inner-core and outer-core regions. On the one hand, the falling of the SLP decreases the surface radial pressure gradient in the inner-core. As a result, the radial wind is weakened according to the radial wind balance and the RMW extends outwards. On the other hand, the low SLP in the outer region increases the radial pressure gradient and enhances the radial wind in the outer region. The wind convergence further enhances the local convection and accelerates the inflow in the outer region. Through this positive feedback, the local tangential wind increases and extends outwards, resulting in a larger TC size (R17).

The size of the TC in the P_SWT is strongly dependent on the distribution of diabatic heating. Further sensitivity experiments were conducted to understand the relative role of circulation and moisture field associated with the SWT in generating stronger convection in the outer region. In the first set of experiments, only specific humidity field associated with the SWT and EW is specified. The experiments indicate that the moisture difference affects the TC generation time. The generation time of the TC in SWT_SH is earlier than EW_SH, and as a result, the TC size is larger. However, the size difference does not alter in the later integration period. In the second set of experiments, only the dynamic field associated with the SWT and EW is specified. Compared with the EW, the surface wind speed of the SWT is larger. Therefore, the SWT generates more moisture in the outer region than EW by evaporation process. Meanwhile, the vertical profile of the divergence field indicated that the ascending motion of the SWT is stronger. Both the factors favor the greater development of convection in the outer region, leading to the increase of TC size. The relative contributions of the moisture and circulation fields associated with the synoptic perturbation on the TC size difference are about 40% and 60% respectively.

In the current study, we focus on the effect of perturbation type on the TC size between WNP and NA. In the authors' previous studies, the effect of background state on the TC

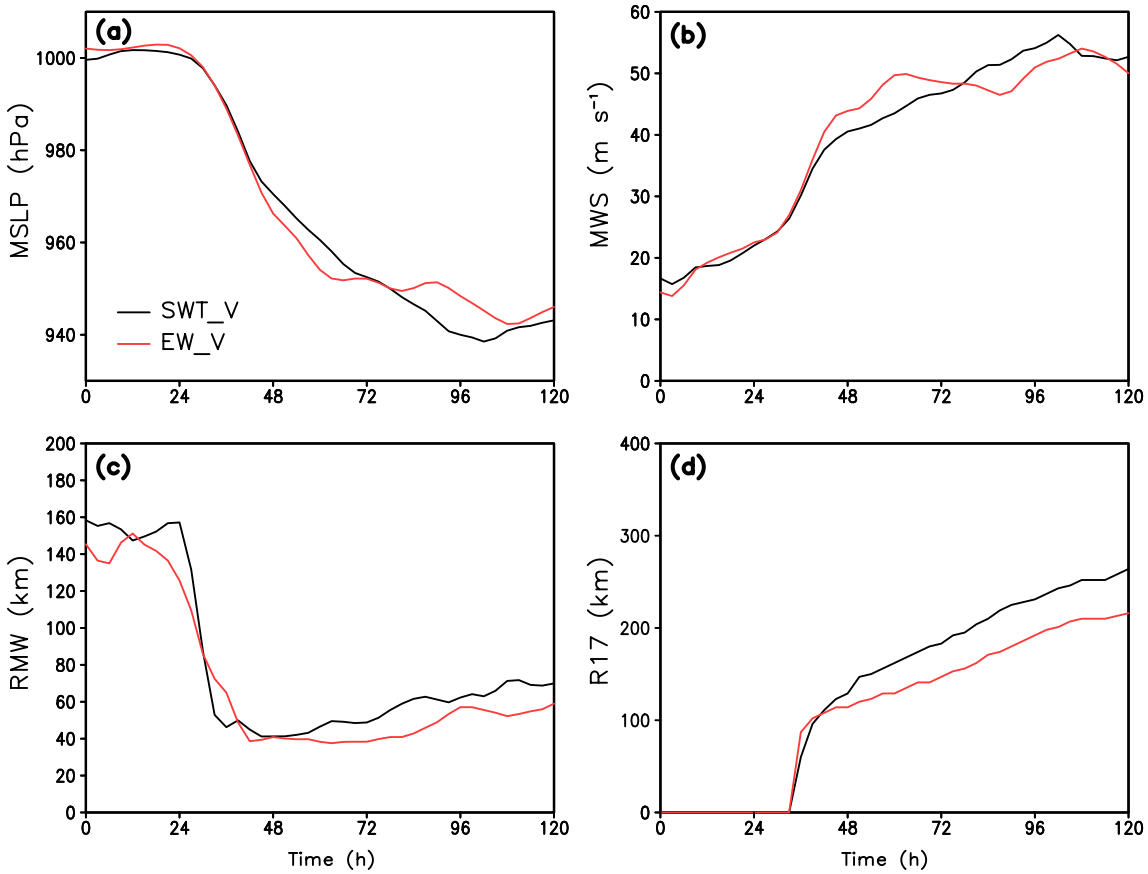

Fig. 10 Time evolutions of **a** MSLP (hPa), **b** MWS (m s^{-1}), **c** RMW (km) and **d** R17 (km) at 10-m height simulated from the SWT_V (black line) and EW_V (red line)

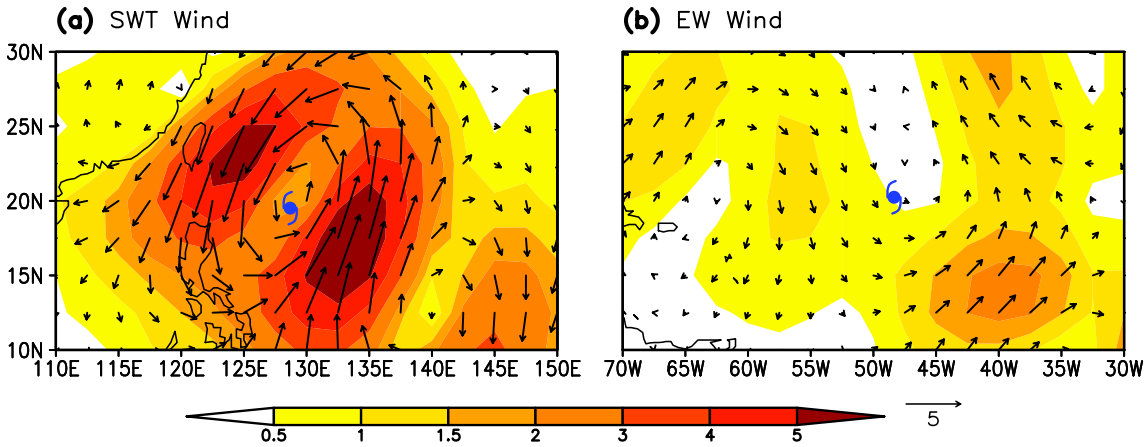

Fig. 11 Horizontal patterns of initial surface wind (m s^{-1}, vector) and wind speed (shaded, m s^{-1}) fields for the **a** SWT and **b** EW composites derived from the observational data. The blue typhoon symbol denotes the location of the initial vortex

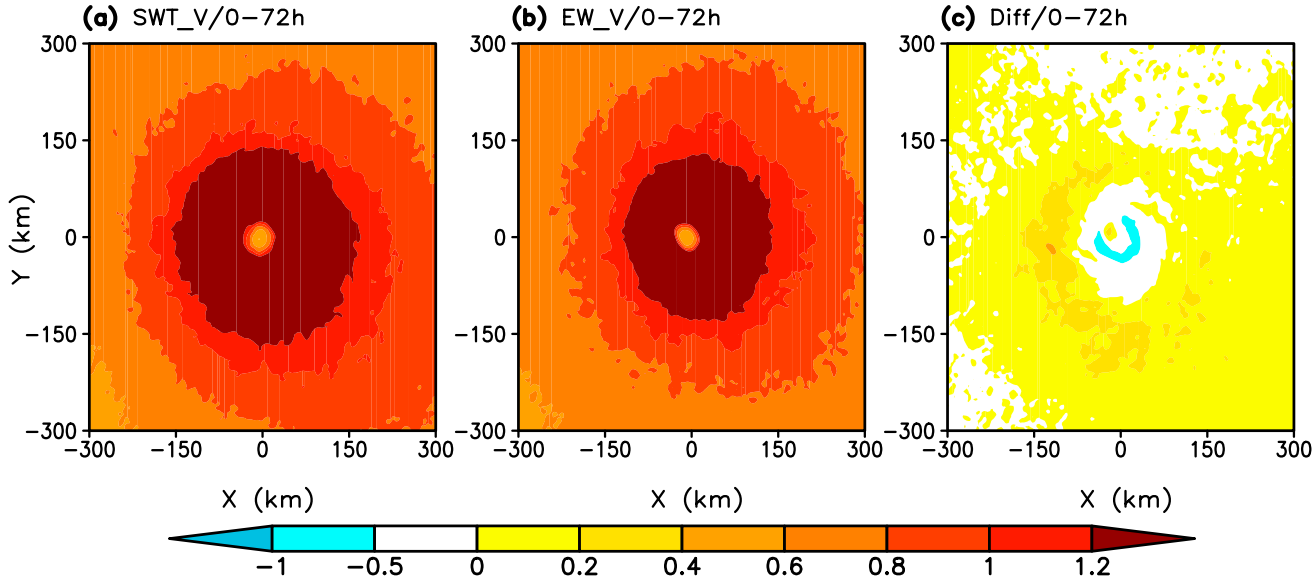

Fig. 12 Horizontal patterns of the upward surface moisture flux (10^{-4} kg m^{-2} s^{-1}) averaged during the first 72 h in **a** the SWT_V and **b** EW_V experiments and **c** their difference (SWT_V—EW_V)

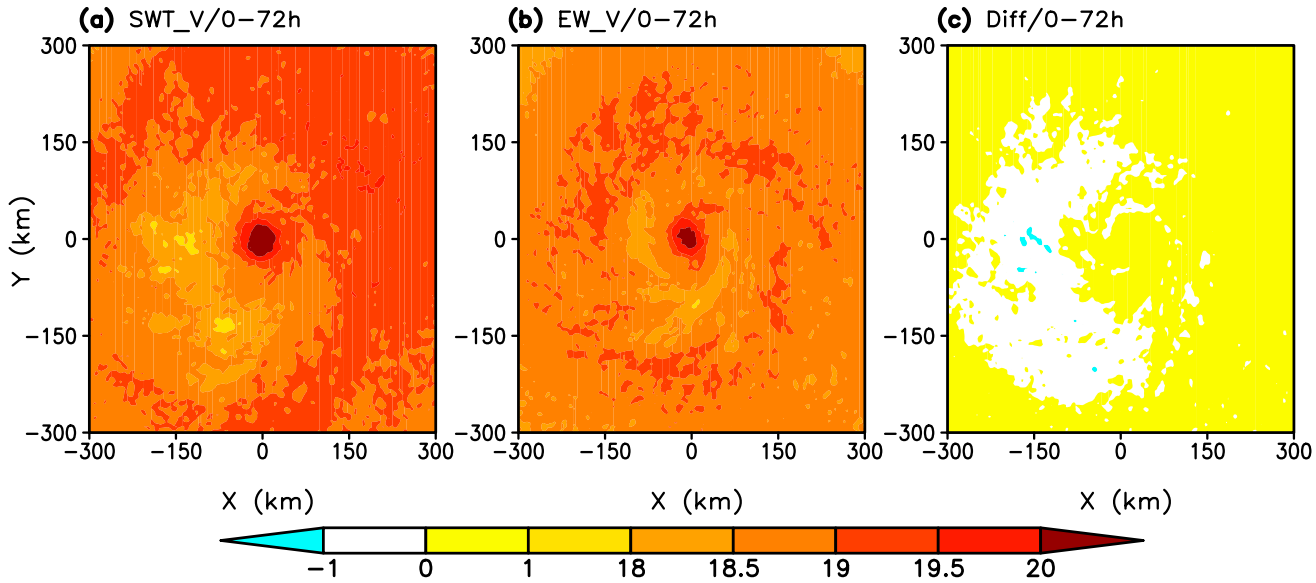

Fig. 13 Horizontal patterns of the near surface specific humidity (g kg^{-1}) averaged during the first 72 h in **a** the SWT_V and **b** EW_V experiments and **c** their difference (SWT_V—EW_V)

size over WNP and NA was investigated (Ma et al. 2019b). An interesting question is which one, the environmental condition or perturbation type, is more important in causing TC size difference between the two basins? The simulation result in Ma et al. (2019b) showed that the background mean state difference counted about 38% difference of TC size between the WNP and NA basin (i.e., reducing 70 km from 184 km in WNP). This ratio is comparable to 31% size difference in the current study (i.e., reducing 77 km from the original TC size of 252 km in WNP) (Fig. 14). The result indicates that both the effects of the background mean state and the perturbation type are important in causing the TC size difference between the WNP and NA basins.

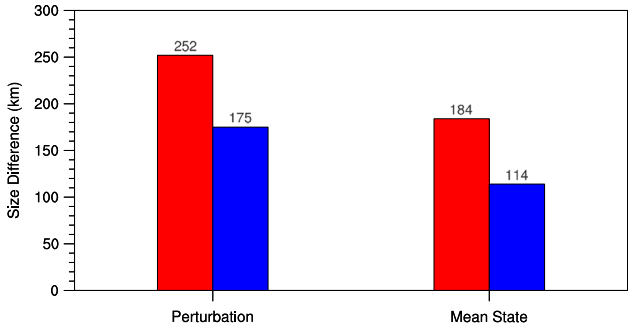

Fig. 14 A comparison of effects of the perturbation type versus the mean state between the WNP (red bar) and NA (blue bar) on tropical cyclone size. Here the effect of the perturbation type is based on P_SWT and A_EW, whereas the effect of the mean state is based on Ma et al. (2019b)

Acknowledgements This study is jointly supported by NSFC Grant 41875069, NSF Grant AGS-16-43297, NOAA Grant NA18OAR4310298, Postgraduate Research & Practice Innovation Program of Jiangsu Province SJKY19_0928 and China Scholarship Council (CSC) under the Grant CSC N201808320282. This is SOEST contribution number 11153, IPRC contribution number 1477 and ESMC number 327.

References

Avila LA (1991) Atlantic tropical systems of 1990. Mon Wea Rev 119:2027–2033

Avila LA, Pasch RJ (1995) Atlantic tropical systems of 1993. Mon Wea Rev 123:887–896

Burpee RW (1972) The origin and structure of easterly waves in the lower troposphere of North Africa. J Atmos Sci 29:77–90

Chan KTF, Chan JCL (2012) Size and strength of tropical cyclones as inferred from QuikSCAT data. Mon Wea Rev 140:811–824. https://doi.org/10.1175/MWR-D-10-05062.1

Chan KTF, Chan JCL (2013) Angular momentum transports and synoptic flow patterns associated with tropical cyclone size change. Mon Wea Rev 141:3985–4007. https://doi.org/10.1175/MWR-D-12-00204.1

Chan KTF, Chan JCL (2018) The outer-core wind structure of tropical cyclones. J Meteor Soc Japan 96(4):297–315

Chang CP, Morris VF, Wallance JM (1970) A statistical study of easterly waves in the western Pacific: July–December 1964. J Atmos Sci 27:195–201

Chavas DR, Emanuel KA (2010) A QuikSCAT climatology of tropical cyclone size. Geophys Res Lett 37:L18816. https://doi.org/10.1029/2010GL044558

Davis C et al (2008) Prediction of landfalling hurricanes with the advanced Hurricane WRF Model. Mon Wea Rev 136:1990–2005. https://doi.org/10.1175/2007MWR2085.1

Dunkerton TJ, Montgomery MT, Wang Z (2009) Tropical cyclogenesis in a tropical wave critical layer: easterly waves. Atmos Chem Phys 9:5587–5646

Emanuel KA (2005) Increasing destructiveness of tropical cyclones over the past 30 years. Nature 436:686–688

Fu B, Li T, Peng MS, Weng F (2007) Analysis of tropical cyclogenesis in the western North Pacific for 2000 and 2001. Wea Forecast 22:763–780

Fu B, Li T, Peng MS, Weng F, Peng MS, Li T, Stevens DE (2012) Developing versus nondeveloping disturbances in the North Atlantic and Western North Pacific: part II: the Western North Pacific. Mon Wea Rev 140(4):1067–1080

Ge X, Li T, Peng M (2013) Tropical cyclone genesis efficiency: mid-level versus bottom vortex. J Trop Meteorol 19(3):197–213

Gray WM (1968) Global view of the origin of tropical disturbances and storms. Mon Wea Rev 96:669–700

Guo X, Tan ZM (2017) Tropical cyclone fullness: A new concept for interpreting storm intensity. Geophys Res Lett 44:4324–4331

Hill KA, Lackmann GM (2009) Influence of environmental humidity on tropical cyclone size. Mon Wea Rev 137:3294–3315

Holland GJ (1997) The maximum potential intensity of tropical cyclones. J Atmos Sci 54:2519–2541

Hong SY, Noh Y, Dudhia J (2006) A new vertical diffusion package with an explicit treatment of entrainment processes. Mon Wea Rev 134:2318–2341. https://doi.org/10.1175/MWR3199.1

Kain JS, Fritsch JM (1993) Convective parameterization for mesoscale models: The Kain-Fritsch scheme. The Representation of Cumulus Convection in Numerical Models, Meteor. Monogr. No. 46. American Meteorological Society, Washington, pp 165–170

Kalnay E et al (1996) The NCEP/NCAR 40-year reanalysis project. Bull Am Meteorol Soc 77:437–471. https://doi.org/10.1175/1520-0477(1996)077%3c0437:TNYRP%3e2.0.CO;2

Landsea CW (1993) A climatology of intense (or major) Atlantic hurricane. Mon Wea Rev 121:1703–1712

Lau K-H, Lau N-C (1990) Observed structure and propagation characteristics of tropical summertime synoptic-scale disturbances. Mon Wea Rev 118:1888–1913

Li T (2006) Origin of the summertime synoptic-scale wave train in the western North Pacific. J Atmos Sci 63:1093–1102

Li T (2012) Synoptic and climatic aspects of tropical cyclogenesis inwestern North Pacific. In: Oouchi K, Fudeyasu H (eds) Cyclones: formation, triggers and control. Nova Science Publishers, Hauppauge, pp 61–94

Li T, Fu B (2006) Tropical cyclogenesis associated with Rossby wave energy dispersion of a preexisting typhoon. Part I: satellite data analysis. J Atmos Sci 63:1377–1389

Li T, Ge X, Wang B, Peng M (2003) Satellite data analysis and numerical simulation of tropical cyclone formation. Geophys Res Lett 30:2122–2126

Li T, Ge X, Wang B, Zhu Y (2006) Tropical cyclogenesis associated with Rossby wave energy dispersion of a preexisting typhoon. Part II: numerical simulations. J Atmos Sci 63:1390–1409

Lin YL, Farley RD, Orville HD (1983) Bulk parameterization of the snow field in a cloud model. J Appl Meteorol 22:1065–1092. https://doi.org/10.1175/1520-0450(1983)022%3c1065:BPOTSF%3e2.0.CO;2

Ma C, Sun Y, Liu J, Li T, Zhong Z (2019) Impact of cumulus parameterization on model convergence of tropical cyclone destructive potential simulation at grey-Zone resolutions: a numerical investigation. Atmosphere 10(2):74

Ma C, Peng M, Li T, Sun Y, Liu J, Bi M (2019) Effects of background state on tropical cyclone size over the Western North Pacific and Northern Atlantic. Clim Dyn 52(7–8):4143–4156

Merrill RT (1984) A comparison of large and small tropical cyclones. Mon Wea Rev 112:1408–1418

Peduzzi P, Chatenoux B, Dao H, De Bono A, Herold C, Kossin J, Mouton F, Nordbeck O (2012) Global trends in tropical cyclone risk. Nat Clim Change 2:289–294

Peng MS, Fu B, Li T, Stevens DE (2012) Developing versus nondeveloping disturbances in the North Atlantic and Western North Pacific: part I: the North Atlantic. Mon Wea Rev 140(4):1047–1066

Pielke RA Jr, Gratz J, Landsea CW, Collins D, Saunders M, Musulin R (2008) Normalized hurricane damage in the United States: 1900–2005. Nat Hazards Rev 9:29–42

Ritchie EA, Holland GJ (1999) Large-scale patterns associated with tropical cyclogenesis in the western Pacific. Mon Wea Rev 127:2027–2043

Rotunno R, Emanuel KA (1987) An air–sea interaction theory for tropical cyclones. Part II: evolutionary study using a nonhydrostatic axisymmetricmodel. J Atmos Sci 44:542–561

Skamarock WC, Coauthors (2008) A description of the Advanced Research WRF version 3. NCAR Tech. Note NCAR/TN-4751STR, 113 pp.

Sun Y, Zhong Z, Li T, Yi L, Hu Y, Wan H, Chen H, Liao Q, Ma C, Li Q (2017) Impact of ocean warming on tropical cyclone size and its destructiveness. Sci Rep 7:8154

Wang YQ (1995) On an inverse balance equation in sigma coordinates for model initialization. Mon Wea Rev 123:482–488

Wang YQ (2001) An explicit simulation of tropical cyclones with a triply nested movable mesh primitive equation model: TCM3. Part I: model description and control experiment. Mon Wea Rev 129:1370–1394

Wang YQ (2009) How do outer spiral rainbands affect tropical cyclone structure and intensity? J Atmos Sci 66:1250–1273

Wang YQ (2012) Recent research progress on tropical cyclone structure and intensity. Trop Cyclone Res Rev 1:254–275

Wang Z, Dunkerton TJ, Montgomery MT (2012) Application of the marsupial paradigm to tropical cyclone formation from northwestward-propagating disturbances. Mon Wea Rev 140:66–76

Wu L, Tian W, Liu Q, Cao J (2015) Implications of the observed relationship between tropical cyclone size and intensity over the western North Pacific. J Clim 28:9501–9506

Xu J, Wang Y (2010) sensitivity of the simulated tropical cyclone inner-core size to the initial vortex size. Mon Wea Rev 138(11):4135–4157

Xu Y, Li T, Peng M (2013) Tropical cyclogenesis in the western North Pacific as revealed by the 2008–2009 YOTC data. Wea Forecast 28:1038–1056

Xu Y, Li T, Peng M (2014) Roles of the synoptic-scale wave train, the intraseasonal oscillation, and high-frequency eddies in the genesis of typhoon manyi (2001). J Atmos Sci 71(10):3706–3722

Yuan J, Li T, Wang D (2015) Precursor synoptic-scale disturbances associated with tropical cyclogenesis in the South China Sea during 2000–2011. Int J Climatol 35:3454–3470